Experimental and numerical evaluation of a ring-shaped emitter for subsurface irrigation

Preprint · October 2018

DOI: 10.1016/j.agwat.2018.09.039

3 authors, including:

Reskiana Saefuddin
Tokyo University of Agriculture and Technology
2 PUBLICATIONS **0** CITATIONS
SEE PROFILE

Hirotaka Saito
Tokyo University of Agriculture and Technology
67 PUBLICATIONS **2,015** CITATIONS
SEE PROFILE

Agricultural Water Management 211 (2019) 111–122

Contents lists available at ScienceDirect

Agricultural Water Management

journal homepage: www.elsevier.com/locate/agwat

Experimental and numerical evaluation of a ring-shaped emitter for subsurface irrigation

Reskiana Saefuddin[a], Hirotaka Saito[a,*], Jiří Šimůnek[b]

[a] Tokyo University of Agriculture and Technology, Fuchu, Tokyo, 183-8509 Japan
[b] University of California, Riverside, CA 92521 USA

ARTICLE INFO

Keywords:
Subsurface irrigation
Ring-shaped emitter
Macroscopic
Capillary length
Water use efficiency (WUE)
Numerical simulation

ABSTRACT

A low-cost subsurface irrigation system can generate benefits for small-scale farmers who have scarce water resources. A ring-shaped emitter made from a standard rubber hose has been developed and introduced for subsurface irrigation in Indonesia. It is a low-cost irrigation technology based on indigenous materials and skills. To build a ring-shaped emitter of the original design, a rubber hose is bent into a ring shape with a diameter of about 20 cm, and then five 5-mm holes are drilled into it at even intervals. Next, the entire ring-shaped hose is covered with a permeable textile so that water can infiltrate in all directions around the buried emitter. Water is applied from a water tank connected to the emitter by adjusting the pressure head imposed at the inlet of the emitter. Although it has been successfully used in practice, the performance of the ring-shaped emitter has not been evaluated in detail. Additionally, because the ring-shaped hose is fully covered with the textile, it may be difficult to detect any malfunctions or repair it. To promote the ring-shaped emitter for subsurface irrigation among small-scale farmers in arid or semi-arid regions, it is important to design an emitter that is easy to maintain. This study proposes a reduction in the number of holes and a change of covering method. Because the number of experiments that can be carried out to evaluate the performance of alternative ring-shaped emitters is usually limited, numerical simulations can be performed in addition to experiments. The main objectives of this study thus were 1) to experimentally investigate the water movement around a buried ring-shaped emitter and 2) to numerically evaluate the effect of modifying the design of the ring-shaped emitter on soil water dynamics around the emitter. Numerical simulations were carried out using HYDRUS, one of the most complete packages for simulating variably-saturated water flow in two- or three-dimensional domains. HYDRUS simulations in a fully three-dimensional domain were performed using the soil hydraulic parameters that were optimized against experimental data collected during experiments with the original ring-shaped emitter. Simulation results confirmed that reducing the number of holes does not significantly affect the water availability in silt for model plants, such as tomato and strawberry, and that covering the entire emitter is not necessary. Partially covering the emitter allows one to maintain the emitter much more easily compared to the original fully-covered emitter.

1. Introduction

Some of the modern irrigation technologies designed for large-scale farming with complex and expensive devices tend to fail when introduced in rural areas of developing countries where farming is generally practiced on a much smaller scale. In these areas, maintaining complex irrigation systems can become a roadblock to promoting modern technologies because there may not be enough well-trained engineers and it may be difficult to find parts to repair these systems. Therefore, the use of indigenous skills and materials is crucial to introducing irrigation technologies in such communities.

Subsurface irrigation with a ring-shaped emitter (Saefuddin et al., 2014) is one of the irrigation techniques recently developed and introduced in rural areas of Indonesia for cultivating annual and perennial crops (e.g., Sumarsono et al., 2018). An emitter made from a rubber hose is economically affordable, especially for small-scale farmers. After a rubber hose is bent into a ring shape with a diameter of about 20 cm, five 5-mm holes are drilled into it at even intervals. An entire ring-shaped hose is then covered with a permeable textile so that irrigation water can be distributed through the permeable textile in all directions around an emitter. When used in the field conditions, a number of ring-shaped emitters can be connected to a pipeline which delivers water from a water source, such as a reservoir, a water tank, or a faucet. A constant pressure head can be maintained at the inlet when

* Corresponding author.
E-mail address: hiros@cc.tuat.ac.jp (H. Saito).

https://doi.org/10.1016/j.agwat.2018.09.039
Received 10 April 2018; Received in revised form 9 August 2018; Accepted 21 September 2018

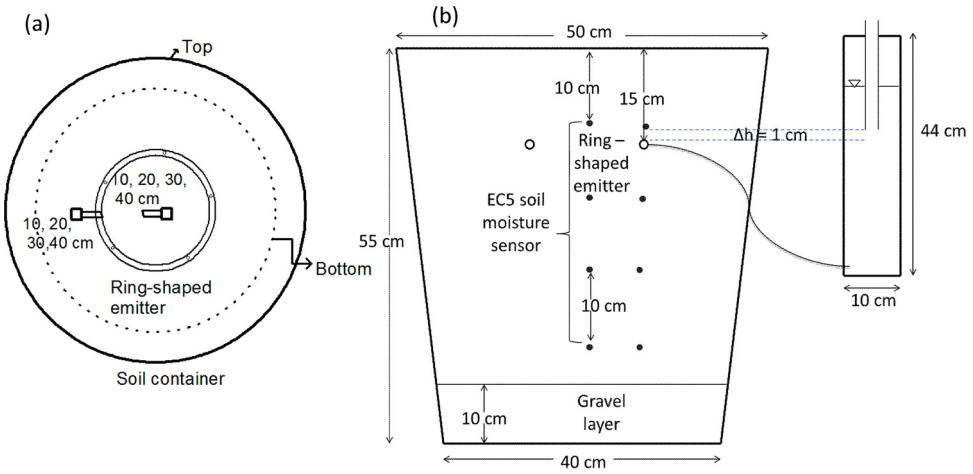

Fig. 1. Top view (a) and cross-section (b) of the soil container used in the laboratory experiments with a ring-shaped emitter.

the emitter is connected to a water tank. Sumarsono et al. (2018) applied 25-cm pressure head to the buried ring-shaped emitter to cultivate annual and perennial crops.

Although ring-shaped emitters have been successfully used for cultivating, for example, melon on an island of Indonesia where precipitation is limited (Saefuddin et al., 2014), its current design and operation are purely empirical. Understanding soil water movement and the spatial extent of the wetted volume around an emitter is crucial to achieving optimum operation of subsurface irrigation with a ring-shaped emitter and to modifying its design to improve usability and water-use efficiency. In addition, the current design of the ring-shaped emitter does not allow one to easily detect malfunctions because the emitter is fully covered with a permeable textile. As a result, it is not easy to repair it quickly.

For faster promotion of the technology, it is important to have a design that is easy to maintain. It has not yet been evaluated whether the number of holes can be reduced and/or whether it is possible to cover emitters only partially with a permeable textile. Because the number of experiments that can be carried out is usually limited, numerical simulations can be used instead to evaluate the performance of ring-shaped emitters of various designs and under different soils and environmental conditions. Using numerical simulations, a design that is more robust may be developed.

In this study, the HYDRUS (2D/3D) model (Šimůnek et al., 2016) was used to simulate soil water movement during subsurface irrigation with a ring-shaped emitter. The model is referred to simply as HYDRUS in the reminder of the manuscript. A number of past studies confirmed the suitability of HYDRUS for simulating water movement during subsurface irrigation. For example, Skaggs et al. (2004) compared HYDRUS-simulated water contents for a subsurface line-source drip irrigation with observed field data for three different emitter discharge rates. Kandelous and Šimůnek (2010b) used HYDRUS to evaluate laboratory and field data involving water movement in clay loam from point water sources buried at different depths and with different discharge rates. Kandelous et al. (2011) validated HYDRUS to simulate water movement from a subsurface drip irrigation system by comparing simulated results with measured soil water contents in several field experiments.

The main objectives of this study were 1) to experimentally investigate the water movement around a buried ring-shaped emitter during irrigation, 2) to validate the capacity of HYDRUS to simulate such water movement, and 3) to numerically evaluate the effects of modified designs of the ring-shaped emitter on soil water dynamics during irrigation. Laboratory experiments were first carried out to monitor changes in the soil water content at different positions during irrigation using the buried original ring-shaped emitter with five drilled holes that were fully covered by a permeable textile. While the emitter was developed to aid plant cultivation, the laboratory experiments were carried out without any plants in this study to avoid any difficulties associated with plant root water uptake. The collected experimental soil moisture data were used to calibrate HYDRUS. The calibrated model was then validated by comparing its prediction against additional experimental data.

The third objective was achieved by simulating changes in the soil water content around buried emitters of different designs. As an indirect quantitative proxy for evaluating the three-dimensional wetted volume around the buried emitter, corresponding root water uptake rates were computed. When water around the emitter is not uniformly distributed, the roots around the buried emitter may not be able to uptake water at an optimum rate because some parts of the root system are under stress. The root water uptake rate, therefore, can be used as an indirect indicator of how buried ring-shaped emitters of different designs performed compared to the original ring-shaped emitter.

2. Materials and methods

2.1. Laboratory experiments with the ring-shaped emitter

The laboratory experiments were carried out using a container (50 cm in diameter at the top, 40 cm in diameter at the bottom, and 55 cm in height) filled with air-dried soil (Fig. 1). Two soil types, silt and sand, were used in the experiments. Soils were packed in 5-cm increments at the predetermined bulk density of 1.41 g cm^{-3} and 1.52 g cm^{-3} for silt and sand, respectively. A 10-cm thick gravel layer was installed at the bottom of the container. For each experiment, the original ring-shaped emitter was installed at a depth of 15 cm. The emitter was connected to a Mariotte tank (10 cm in diameter and 44 cm in height) to control the water pressure head applied at the inlet (referred to as the inlet pressure). In this study, a constant pressure head of either 1 cm or 5 cm was maintained at the inlet of the buried emitter for 10 h to apply water through the emitter. Although a much higher pressure head was imposed at the inlet in field cultivation practices (e.g., Sumarsono et al., 2018), either 1 cm or 5 cm was used in this experiment to avoid a positive back pressure at the outlets (Shani et al., 1996; Lazarovitch et al., 2005). During the experiments, the volume of water in the Mariotte tank was recorded every 30 min to obtain the water application rate (i.e., the emitter discharge rate).

The ring-shaped emitter used in this study was made from a rubber water hose. The hose, which had a 1 cm inner diameter, was bent into a ring shape with a diameter of about 20 cm. There were 5 small holes with 0.5 cm in diameter drilled at even intervals on one side of the ring. The entire ring was covered with a permeable textile so that applied

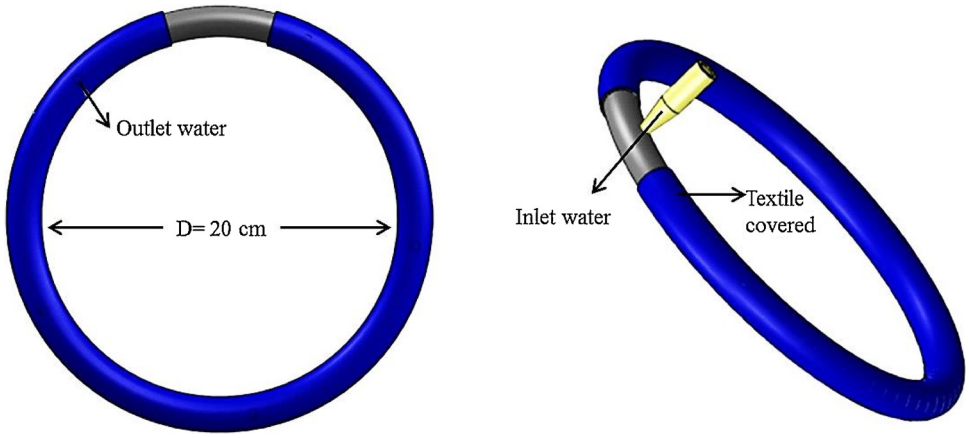

Fig. 2. Schematic of the original ring-shaped emitter used in the laboratory experiment.

water could infiltrate in all directions into the soil. The original ring-shaped emitter is referred to as the 5 F emitter in the remainder of the manuscript. The schematic of the ring-shaped emitter is depicted in Fig. 2. When the ring-shaped emitter was installed in the soil, its 5 holes were all facing down to block any soil particles from entering the holes.

There were 8 capacitance soil moisture sensors, EC5, a product of METER Environment, installed around the buried emitter to monitor changes in the soil water content. Fig. 1 shows the position of the sensors in the container. Four sensors were installed at depths of 10, 20, 30, and 40 cm directly above and below the emitter and four additional sensors were installed at the same depths in the center of the emitter. Since the ring-shaped emitter was installed at a depth of 15 cm, the four sensor installation depths were 5 cm above, and 5, 15, and 25 cm below the emitter, respectively. The soil moisture sensors were individually calibrated for the soils used in the experiments. Soil water retention data for the sand and silt soil were determined using a suction plate and a pressure plate apparatus. The van Genuchten-Mualem model was fitted to the data using the RETC software package (van Genuchten et al., 1991).

2.2. Root water uptake mode in HYDRUS

In this study, HYDRUS was used to simulate water movement in soil during subsurface irrigation with a ring-shaped emitter. In HYDRUS, root water uptake is modeled as a sink term in the Richards equation using the stress response function proposed by Feddes et al. (1978). A compensated root water uptake model is also implemented by introducing a threshold value, referred to as the root adaptability factor, of a dimensionless water stress index, which is defined as the ratio of actual and potential transpiration (Šimůnek and Hopmans, 2009). If the water stress index is above the root adaptability factor, reduced root water uptake in one part of the root zone is fully compensated for by root water uptake from other parts of the root zone where the water stress is smaller, so that the actual transpiration rate is equal to the potential transpiration rate. If the water stress index is below the root adaptability factor, reduced water uptake is only partially compensated. The ratio of actual to potential transpiration is then equal to the ratio of the water stress index to the root adaptability factor, which is less than unity. In this study, the compensated root water uptake model with the root adaptability factor of 0.25 was used when comparing different configurations of the ring-shaped emitter.

The following three-dimensional root distribution function $b(x, y, z)$ of Vrugt et al. (2001) is implemented in HYDRUS :

$$b(x,y,z) = \left[1-\frac{x}{X_m}\right]\left[1-\frac{y}{Y_m}\right]\left[1-\frac{z}{Z_m}\right]e^{-\left(\frac{p_x}{X_m}|x^*-x|+\frac{p_y}{Y_m}|y^*-y|+\frac{p_z}{Z_m}|z^*-z|\right)} \quad (1)$$

where X_m, Y_m, and Z_m are the maximum rooting lengths in the x, y, and z directions [L], respectively, and P_x [-], P_y [-], P_z [-], x^* [L], y^* [L], and z^*[L] are empirical parameters. These empirical parameters are included to account for asymmetrical root water uptake in any direction and to allow for a maximum root water uptake at any location (X_0, Y_0, Z_0) where ($0 < X_0 < X_m$, $0 < Y_0 < Y_m$, $0 < Z_0 < Z_m$). Following Vrugt et al. (2001), P_x, P_y, and P_z were all set to unity for $x > x^*$, $y > y^*$, and $z > z^*$. More details about HYDRUS can be found in Šimůnek et al. (2011, 2016) and Radcliffe and Šimůnek (2010).

2.3. Soil hydraulic parameter estimation

HYDRUS also has the ability to inversely estimate soil hydraulic parameters from transient variably-saturated water flow data, such as from water flow data collected during subsurface water application experiments with the original-design ring-shaped emitter. The inverse method implemented in HYDRUS is based on the minimization of an objective function, which expresses the discrepancy between observed and predicted water flow variables. HYDRUS uses the Marquardt-Levenberg optimization algorithm (Marquardt et al., 1963) to minimize the objective function. In this study, a soil hydraulic parameter set that minimizes the objective function given below was estimated. The objective function O was defined as the sum of two components:

$$O(\boldsymbol{\beta}, \boldsymbol{\theta}, \mathbf{q}) = \sum_{j=1}^{m_\theta} v_j \sum_{i=1}^{n_{\theta j}} w_{i,j}\left[\theta_j^*(\mathbf{x}, t_i) - \theta_j(\mathbf{x}, t_i, \boldsymbol{\beta})\right]^2 + \sum_{k=1}^{n_q} w_k\left[q_c^*(t_k) - q_c(t_k, \boldsymbol{\beta})\right]^2 \quad (2)$$

where θ_j is the soil water content (SWC) at the sensor position $\mathbf{x}$ and q_c is the cumulative emitter discharge at the inlet of the buried ring-shaped emitter [L^3T^{-1}]. The superscript * represents specific measurements at time t_i for SWCs and t_k for the cumulative discharge. While m_θ is the number of sensor locations, $n_{\theta j}$ is the number of measurements at each sensor position. In this objective function, $\theta_j(\mathbf{x}, t_j, \boldsymbol{\beta})$ and $q_c(t_k, \boldsymbol{\beta})$ are the corresponding model predictions for the vector of optimized soil hydraulic parameters, $\boldsymbol{\beta}$, and v_j, $w_{i,j}$, and w_k are weights associated with a particular measurement. During parameter estimation, the selected parameters of the van Genuchten-Mualem model (van Genuchten, 1980) were optimized.

Since the original ring-shaped emitter used in the experiment was fully covered by a permeable textile, we assumed that water infiltrated through the textile in all directions. Therefore, the system could be modeled as an axisymmetrical three-dimensional domain. The domain geometry used in the axisymmetrical three-dimensional model is shown in Fig. 3. Similar axisymmetric modeling approaches have been used in many other studies with a subsurface point water source (Cote et al.,

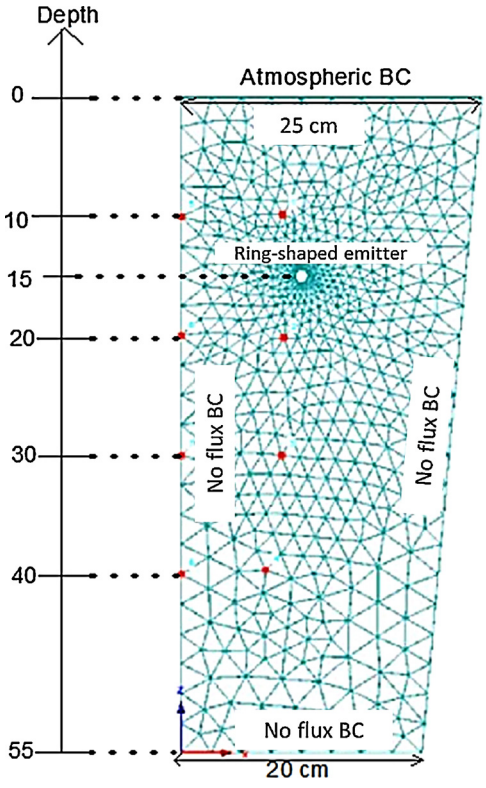

Fig. 3. An axisymmetric three-dimensional simulation domain used in the numerical analysis of water flow from a buried ring-shaped emitter. Eight red dots in the domain depict positions of moisture sensors. (For interpretation of the references to colour in this figure legend, the reader is referred to the web version of this article).

2003; Gärdenäs et al., 2005; Provenzano, 2007; Kandelous and Šimůnek, 2010a; Kandelous et al., 2011; Naglič et al., 2014). A circle with a 1-cm diameter located at a 15-cm depth in the domain represents the cross-section of the buried ring-shaped emitter (Fig. 3). The entire flow domain was discretized into 661 nodes and 1246 triangular finite elements, with their sizes gradually increasing away from the emitter. The finite element mesh was generated using an automatic triangulation algorithm that is implemented in HYDRUS. Changes in the soil water content through time were simulated at 8 observation nodes that corresponded with the positions of the soil moisture sensors installed as shown by red dots in Fig. 3. The observed average initial water content (θ_{in}) was assigned to the entire flow domain as the initial water content. The average initial water contents were $0.044\ cm^3\ cm^{-3}$ and $0.046\ cm^3\ cm^{-3}$ for silt and sand, respectively. The van Genuchten-Mualem model parameters fitted to experimental retention curves were used as initial estimates of optimized parameters. As for K_s, the values provided in the ROSETTA Soil Catalog (K_s = 29.7 cm h^{-1} for sand and 0.35 cm h^{-1} for silt) were used as initial estimates.

While an atmospheric boundary condition was used at the soil surface, no flux boundary conditions were used at the bottom and both sides of the domain during the simulation. As for the nodal points along the perimeter of the emitter, a boundary condition that changes from a constant pressure head condition to a no flux condition at a specified time was used. This boundary condition is referred to in HYDRUS as the time-variable flux/head boundary condition. While a constant pressure head equal to the pressure head imposed during the laboratory experiment was used in nodes along the emitter during the water application time (the first 10 h), a no-flux boundary condition was used after the water application was stopped (after 10 h). This boundary condition applies a specified pressure head to the lowest nodal point of the emitter and adjusts pressure heads in the other nodal points based on the vertical coordinates.

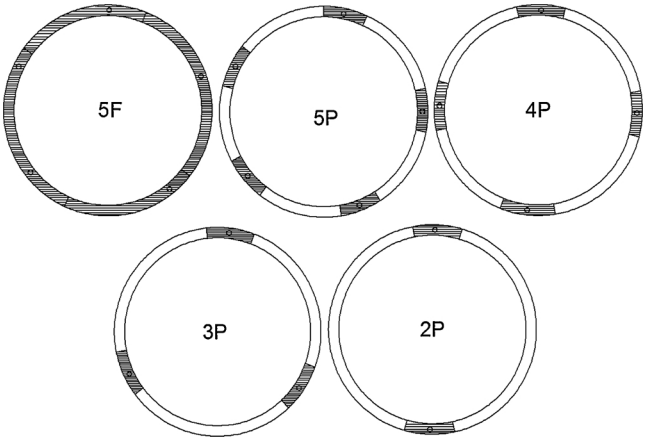

Fig. 4. Schematics (top views) of ring-shaped emitters of different designs. Black sections depict locations of holes covered with permeable textile and white sections depict rubber hoses without cover (i.e., impermeable parts).

2.4. Numerical analysis of alternative emitter configurations

One of the main objectives of this study was to numerically investigate the effect of changing ring-shaped emitter configurations, especially the number and locations of holes and the textile cover, on the spatial extent of the wetted volume around the buried emitter. In addition to the original ring-shaped emitter with five drilled holes fully covered by a permeable textile, ring-shaped emitters with a reduced number of holes and only partially covered by the textile were considered. Modified emitters with 2, 3, 4, and 5 holes, referred to as 2 P, 3 P, 4 P, and 5 P emitters, respectively, were considered in this study. The original ring-shaped emitter is referred to as 5 F. Fig. 4 shows a top view of the five different ring-shaped emitters considered in this study. The black sections of the ring represent the locations covered with the textile (i.e., permeable sections), while the white sections represent the ring without the textile (i.e., impermeable sections). The partially covered emitters were designed to increase the ease of inspection and maintenance.

The numerical simulations were carried out in a fully three-dimensional domain so that the asymmetry in the hole configurations could be modeled without any simplifications. The three-dimensional simulation domain was discretized into 41,016 three-dimensional triangular prismatic elements with finer elements around the emitter (with sizes of 1 cm) and gradually increasing element sizes farther from the emitter (up to 2.5 cm). The initial and boundary conditions of these simulations were similar to those used in the axisymmetrical three-dimensional case. The time-variable flux/head boundary condition was specified in the nodes representing the ring with the textile (dark blue parts in Fig. 4). The inlet pressure head was kept constant at 1 cm during the water application in all simulations following the experimental setup. If a much higher inlet pressure head is applied at the inlet, a positive back pressure may build up at the outlets of the emitter, which can lead to a substantial decrease in the emitter discharge rate (Shani et al., 1996). In this numerical analysis, the water application was stopped when the predefined amount of water (e.g., 720 cm^3 per day), which meets the plant water requirement, was injected. The effect of the emitter design was first assessed by simulating changes in the soil water content over 24 h after 720 cm^3 of water was applied to initially dry soils.

In practice, it is important to know the effect of preceding irrigations on the soil water dynamics during subsurface irrigation with the ring-shaped emitter. The simulations were thus also carried out for 504 h (i.e., 21 days), during which water was applied 7 times (i.e., 7

irrigation cycles). In this numerical analysis, water was applied every three days (i.e., at 0, 72, 144, 216, 288, 350, 412, and 484 h from the start of simulation). The amount of water applied during each irrigation cycle matched the cumulative potential transpiration of the model plants over 3 days. The inlet pressure head was again kept constant at 1 cm during the water application.

The comparison of wetted volumes around the buried ring-shaped emitters of different designs is not straightforward in the case of three-dimensional simulations. Calculated water contents at particular locations cannot provide sufficient information on the spatial extent of the wetted volumes. In this study, the effect of different emitter designs on the spatial extent of the wetted volume was assessed using the soil water stress a plant would have been exposed to. Assuming that the plant roots are distributed symmetrically around the buried ring-shaped emitter, a non-uniformity in the spatial extent of the wetted volume may cause stress to the plant roots. For example, when some parts of the soil are too dry, the plant roots in these regions cannot uptake water at an optimum rate. The uncompensated root water uptake model was first used to indirectly assess the non-uniformity of the spatial extent of the wetted volume around the buried emitter. The compensated root water uptake model was then used to assess whether such non-uniformity would affect actual plant root water uptake.

Two model plants, tomato and strawberry, were considered in this study because of their contrasting spatial root distributions. It has to be mentioned that both crops are known for their high profitability as it is especially important to investigate the effectiveness of subsurface irrigation with the ring-shaped emitter for highly profitable crops. Fig. 5 shows the spatial root distribution defined using the Vrugt's model for both tomato and strawberry. The spatial root distribution was considered constant with time during simulations (i.e., the root growth was neglected). While Table 1 summarizes the spatial root distribution parameters for tomato and strawberry, Table 2 lists the corresponding parameters of the stress response functions. These values were modified from those available in HYDRUS to improve the computational stability. The simulations were carried out for two soil textures: silt and sand. A typical potential evapotranspiration (T_p) rate of 6 mm d^{-1}

Table 1
Parameters describing the spatial root distribution of two model plants (tomato and strawberry) using the Vrugt model (Vrugt et al., 2001).

Parameters	Tomato	Strawberry
Maximum rooting depth, Z_m (cm)	40	30.5
Depth with maximum root density, z^* (cm)	25	5
Maximum rooting radius, X_m (cm)	20	20
Radius of Maximum intensity, x^* (cm)	0	0
Maximum rooting radius, Y_m (cm)	20	20
Radius of maximum intensity, y^* (cm)	0	0
Non-symmetry coefficient, P_z, P_x, and P_y	1, 1, 1	1, 1, 1
Surface area associated with transpiration (cm^2)	1200	1200

Table 2
The modified parameters for the stress response function of Feddes et al. (1978) for tomato and strawberry.

Threshold parameters	Value
Tomato	
h_1 (cm)	−10
h_2 (cm)	−20
h_3 (cm)	−100
h_4 (cm)	−150
Strawberry	
h_1 (cm)	−10
h_2 (cm)	−20
h_3 (cm)	−150
h_4 (cm)	−200

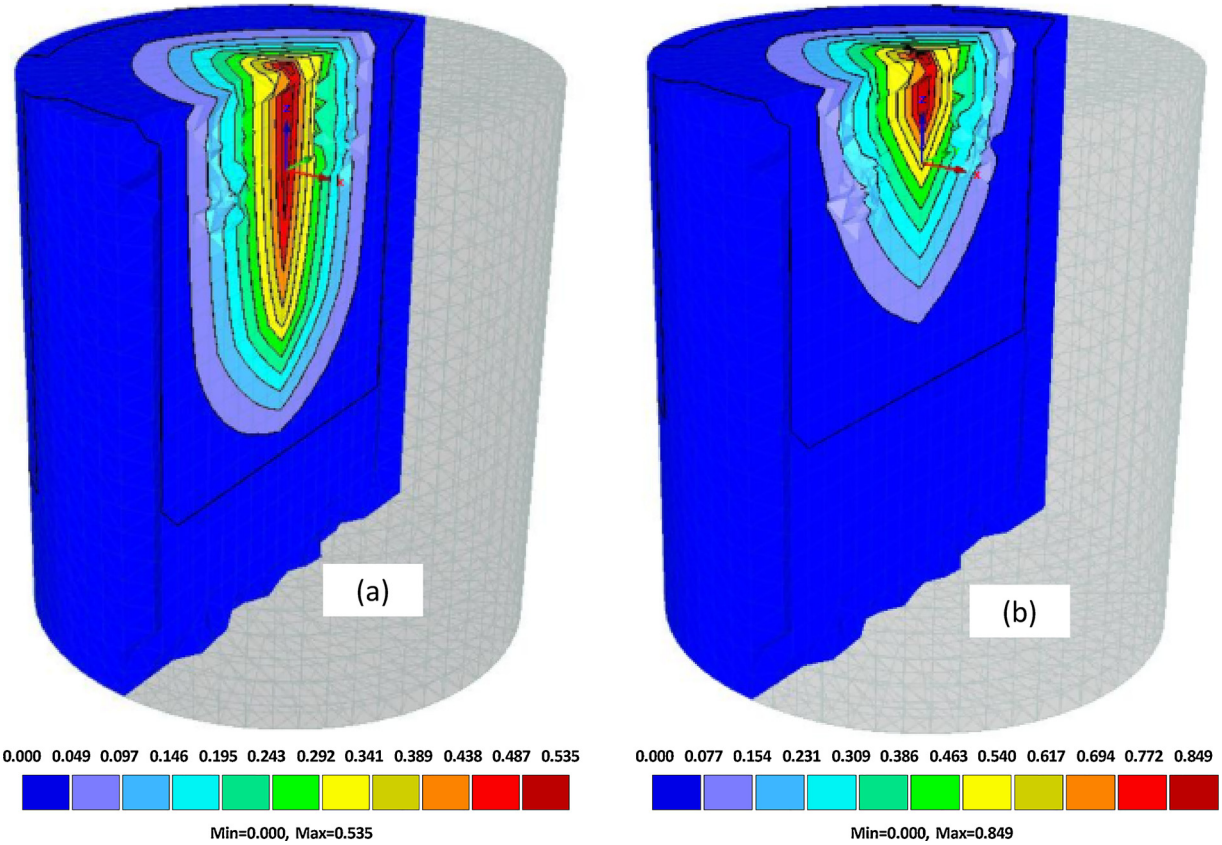

Fig. 5. Spatial root distributions based on the Vrugt's model (Vrugt et al., 2001) for a) tomato and b) strawberry in a three-dimensional simulation domain. Different colors depict different root densities.

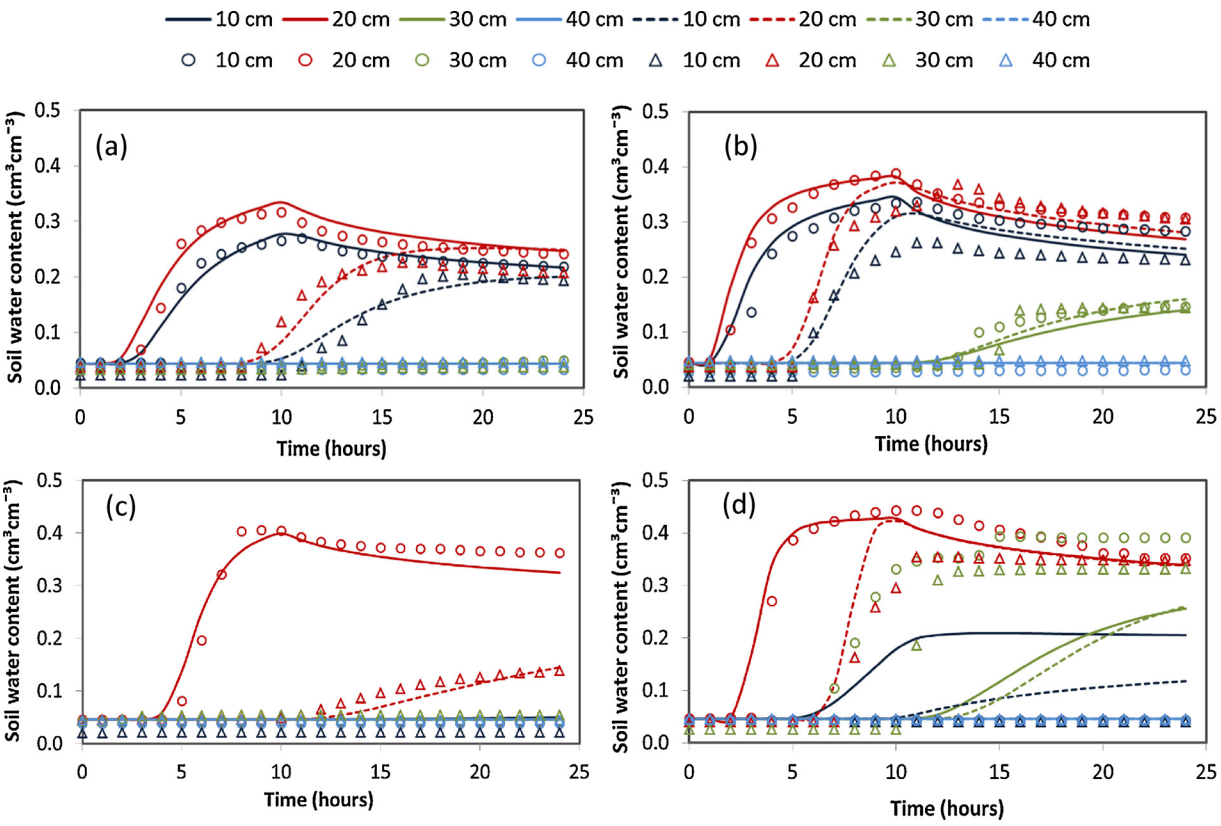

Fig. 6. Soil water contents (SWCs) measured by 8 moisture sensors positioned in 4 depths (10, 20, 30, and 40 cm from the soil surface) during the subsurface water application experiments in silt (a and b) and sand (c and d). Open circles depict SWCs observed at the positions directly above (i.e., 5 cm above) and below (i.e., 5, 15, and 25 cm below) the emitter (installed at a 15-cm depth), whereas open triangles show SWCs observed at the corresponding depths in the center of the soil container. Two different inlet pressure heads (i.e., 1 cm (a and c) and 5 cm (b and d)) were applied during the experiments. Lines depict corresponding SWCs simulated using HYDRUS. While HYDRUS was calibrated using the data collected with the 1-cm inlet pressure head (a and c), it was validated using the data observed with the 5-cm inlet pressure head (b and d).

(Shani et al., 2007), which corresponds to 720 cm^3 of water per day, was used in the analysis. Simulations were carried out using the soil hydraulic parameters inversely estimated as described in Section 2.3. The ring-shaped emitter was placed in a depth of 15 cm, similarly as during the experiment.

3. Results and discussions

3.1. Laboratory experiments

Subsurface water application experiments were carried out using the original ring-shaped emitter (5 F) on two different soils: silt and sand. Fig. 6 depicts soil water contents (SWCs) observed at 8 locations. Fig. 7 observed cumulative discharge rates as a function of time for two applied inlet pressure heads (1 and 5 cm) and two soils. Open triangles in Fig. 6 show SWCs at the center of the buried ring-shaped emitter in four depths (i.e., 10 cm, 20 cm, 30 cm, and 40 cm), whereas open circles show SWCs directly below and above the buried ring-shaped emitter in the same four depths.

For silt, SWCs 5 cm directly below and above the buried ring-shaped emitter (i.e., 10 and 20 cm depths) increased a few hours after the beginning of the water application for both inlet pressure heads. This indicates that water infiltrated radially in all directions around the buried emitter regardless of the inlet pressure head applied. SWCs increased earlier and faster when the inlet pressure head of 5 cm was applied compared to those with the 1 cm inlet pressure head. An initially steep increase in SWCs became more gradual after a few hours, before finally reaching their maximum values after about 10 h at the time when the application of water stopped. An increase in SWCs 5 cm directly below the emitter increased faster than SWCs observed at 5 cm directly above the emitter regardless of the inlet pressure applied because the gravitation enhanced the flow in the downward direction. During the redistribution process, SWCs gradually decreased at both locations. On the other hand, SWCs in the same depths (5 cm above and below the buried emitter) at the center of the buried emitter started increasing much later due to the lateral distance from the emitter (i.e., the water source). As expected, SWCs 5 cm below the emitter increased much faster than those 5 cm above the emitter. When the inlet pressure head was 1 cm, SWCs at the center kept increasing but never reached the same peaks as above and below the emitter at both depths. SWCs at other depths (i.e., 30 and 40 cm below the surface) never increased during the experiment.

The main difference between silt and sand was that observed SWCs did not increase 5 cm above the buried emitter (dark blue symbols in Figs. 6 cd for the depth of 10 cm) in sand. Additionally, when the applied inlet pressure head was 5 cm, increases in SWCs 5 cm and 15 cm below the buried emitter (i.e., in depths of 20 and 30 cm) were especially large. These results indicate that downward water movement was dominant in the sand profile while water moved more radially, including lateral and upward directions, from the emitter in the silt profile. This difference can be attributed to different macroscopic capillary lengths, λ_c, given below, of these two soils (Radcliffe and Šimůnek, 2010).

$$\lambda_c = \frac{\int_{h_i}^{h_0} K(h)dh}{K(h_0) - K(h_i)}$$

The macroscopic capillary length λ_c can be interpreted as the measure of the effects of capillarity as opposed to gravity. The macroscopic

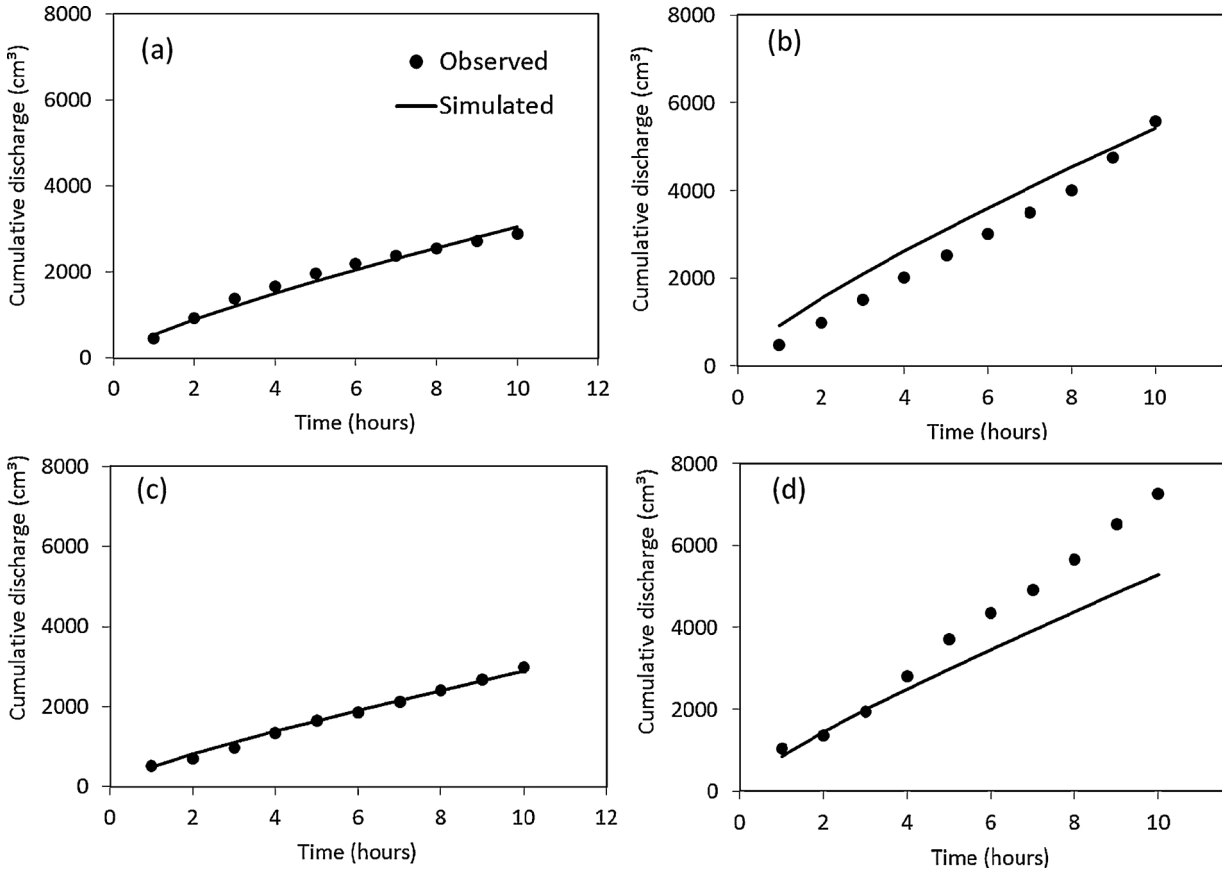

Fig. 7. Observed (dots) and simulated (line) cumulative irrigations for silt (a and b) and sand (c and d) for the applied inlet pressure heads of 1 cm (a and c) and 5 cm (b and d). The data collected using the 1-cm inlet pressure head were used for model calibration, the data collected using the 5-cm inlet pressure head were used for model validation.

capillary length was 7.56 cm and 5.27 cm for silt and sand, respectively, when integrating from $h_i = 0$ cm to $h_0 = -200$ cm. Since sand typically has a much lower macroscopic capillary length than other soils, water flowing from a source will move much less laterally or upward than downward.

The cumulative discharge increased almost linearly for both soils when the applied inlet pressure head was 1 cm. There was no obvious difference in the cumulative discharge between silt and sand. When the inlet pressure increased to 5 cm, while the cumulative discharges for both soils increased almost linearly with time, the cumulative discharge after 10 h of water application in sand was much larger than in silt.

3.2. Model calibration

To calibrate the HYDRUS model for the analysis of water movement during the subsurface water application from the buried ring-shaped emitter, the experimental data observed with the 1-cm inlet pressure head were used. The data collected during the experiments performed with the 5-cm inlet pressure head were then used to validate HYDRUS with calibrated parameters. The soil hydraulic parameters were optimized for both soils by minimizing the objective function given by Eq. (2). Table 3 lists the optimized van Genuchten-Mualem parameters for the sand and silt, while Table 4 summarizes statistics of discrepancies between observations and simulations. For both soils, fitted values of SWCs and cumulative discharges agreed reasonably well with observed values. Both SWRCs and unsaturated hydraulic conductivity functions shown in Fig. 8 agree well with the common shape of the typical curves for both silt and sand (e.g., Jury and Horton, 2004).

The optimized soil hydraulic parameters were then used in HYDRUS to compare simulated and observed SWCs at 8 sensor positions and the cumulative discharges during the experiments performed with the inlet pressure head of 5 cm for both soils. Table 4 summarizes also errors between observations and predictions for simulations with the optimized parameters for experiments with the inlet pressure head of 5 cm. Figures 6bd show both observed and predicted SWCs at 8 sensor positions, whereas Figures 7bd show both observed and predicted

Table 3
The van-Genuchten-Mualem model (van Genuchten, 1980) parameters optimized for silt and sand. Both saturated and residual water contents are marked with * as they were not optimized during the inverse modeling.

Parameters	θ_r*	θ_s*	α	n	K_s (cm/h)	l
Silt (Initial)	0.034	0.400	0.249	2.992	0.35	0.50
Silt (Optimized)	0.034	0.400	0.041	1.734	0.215	0.50
Sand (Initial)	0.045	0..430	0.012	2.421	29.7	0.50
Sand (Optimized)	0.045	0.430	0.137	2.421	0.38	4.09

Table 4
Summary statistics between simulated and observed soil water contents (SWC) at 8 locations where the soil moisture sensors were installed. RMSE, ME, MAE, respectively, are root mean square error, mean error, and mean absolute error computed between simulated and observed SWC.

Soil	Inlet pressure head (cm H_2O)	RMSE ($cm^3\,cm^{-3}$)	ME ($cm^3\,cm^{-3}$)	MAE ($cm^3\,cm^{-3}$)
Silt	1	0.019	−0.057	0.011
	5	0.026	0.038	0.015
Sand	1	0.015	−0.002	0.009
	5	0.061	−0.016	0.032

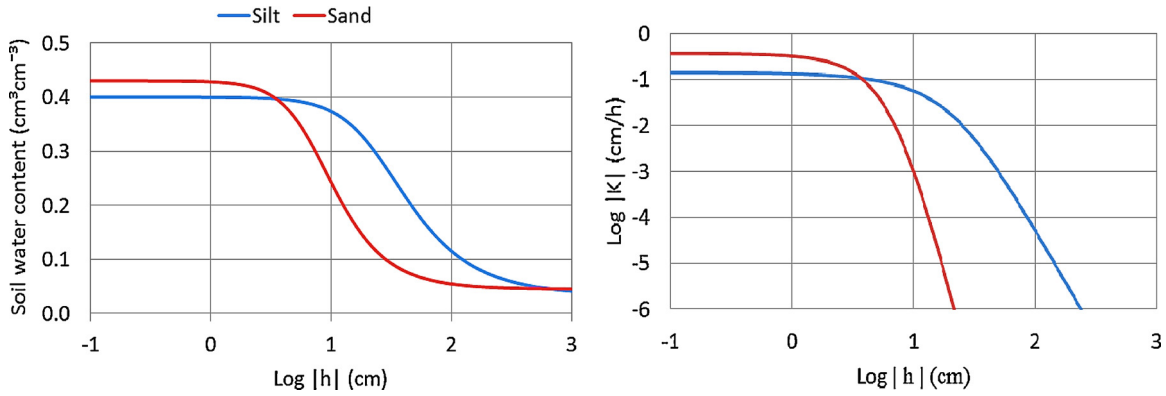

Fig. 8. Soil water retention curves (left) and unsaturated hydraulic conductivity functions (right) for silt and sand described using the van Genuchten-Mualem model with optimized parameters.

cumulative discharges. For silt, both SWCs and cumulative discharges were predicted well using the optimized parameters. For sand, however, predicted SWCs did not agree well with observed ones, especially 15 cm directly below (i.e., in the depth of 30 cm) where SWCs were overestimated and 5 cm directly above (i.e., in the depth of 10 cm) where SWCs were underestimated. This indicates that more downward water flow occurred during the experiment than predicted by the HYDRUS simulation. When the applied inlet pressure head was 5 cm, the preferential-type flow may have occurred underneath the drilled holes of the emitter that enhanced downward water movement. This type of flow clearly creates a non-uniform asymmetrical wetted volume around the buried emitter, which may not be an ideal situation for plant roots to uptake water. Sand is known to be susceptible to preferential flow or finger-type flow when it is initially dry. In places where preferential flow paths are formed, the soil becomes strongly wettable, increasing its ability to conduct water downward through these pathways (Dekker and Ritsema, 1994). It may, therefore, not be a good idea to apply a high inlet pressure when a ring-shaped emitter is installed in an initially dry sandy soil profile.

Fig. 9 shows the spatial extent of the simulated wetted areas around the buried emitter in the axisymmetrical three-dimensional domain after 1, 5, 10, 15, 20, and 24 h using the optimized soil hydraulic parameters listed in Table 3. For each soil, the wetted area (i.e., the wetted volume) was larger when the inlet pressure head was higher. The higher water content around the emitter may cause positive pressure heads building up around the outlets of the emitter that can eventually lead to a decrease in the emitter discharge rate. As expected, while in silt the wetted area expanded radially with time during the water application (i.e., during the first 10 h), downward water movement clearly outpaced lateral or upward movement in the sand profile. These results can again be explained by the differences in the soil hydraulic characteristics, especially the macroscopic capillary length, λ_c, of the two soils used. This study clarified that HYDRUS is indeed a useful tool for analyzing soil water dynamics during the water application with the buried ring-shaped emitter (i.e., subsurface irrigation), as also indicated by a number of other subsurface drip irrigation studies (Bufon et al.,2012; Lazarovitch et al.,2007; Kandelous et al., 2012; El-Nesr et al., 2014; Ghazouani et al., 2015).

3.3. The effect of alternative emitter designs on soil water dynamics

The effects of changing the ring covering method and reducing the number of holes on the spatial extent of the wetted volume around the buried ring-shaped emitter were numerically investigated using HYDRUS. The optimized soil hydraulic parameters listed in Table 3 were used in this analysis. Root water uptake (RWU) was computed as an indirect, quantitative proxy measure to evaluate the spatial extent of the wetted volume. As described in Section 2.4, five different emitter configurations were compared (5 F, 5 P, 4 P, 3 P, and 2 P).

Fig. 10 shows simulated cumulative discharges as a function of the elapsed time for different emitter designs computed over 24 h for initially dry silt and sand when 720 cm^3 of water was applied. For both soils, as expected, the duration needed to reach the same infiltration amount depended strongly on the number of holes. As the number of holes decreased, the duration increased. Although these simulation results show almost constant discharge rates regardless of the emitter design, it has to be mentioned that the emitter discharge rate during subsurface irrigation cannot be kept constant in practice unless a compensated emitter is used.

Fig. 11 shows simulated uncompensated (top) and compensated (bottom) cumulative root water uptake (RWU) of tomato over 24 h in the silt (left) and sand (right) profiles for different ring-shaped emitters. Fig. 12 summarizes the results shown in Fig. 11 for tomato, as well as for strawberry (which were not shown in Fig. 11), using the water use efficiency (WUE), which can be computed as the ratio of cumulative RWU to cumulative irrigation at 24 h. Uncompensated RWU was used as an indirect, quantitative proxy measure of the non-uniformity in the wetted volume around the buried emitter. Compensated RWU was then computed to investigate whether such non-uniformity has any effect on actual plant RWU.

Although uncompensated cumulative RWU in silt increased more slowly when the number of holes was reduced, cumulative uncompensated RWU was almost the same at the end of the simulation for all emitter designs (Fig. 11a). Even though the wetted volume expanded more slowly with the smaller discharge rate in silt when the number of holes was smaller, uncompensated RWU eventually caught up with those for more holes as the wetted volume evolved radially in all directions (as can also be seen in Fig. 9). As for sand, the initial trend is basically the same as for silt; the higher the number of holes, the higher uncompensated RWU. However, uncompensated RWU computed for the 3 P or 2 P emitters in sand, unlike in silt, could not catch up with those for 5 F, 5 P, or 4 P after the water application was stopped. It was also observed that the 5 F emitter had slightly smaller cumulative RWU after 24 h compared to emitters that were partially covered (i.e., 5 P and 4 P). When a ring-shaped emitter with only a small number of holes is used in the sand profile, applied water tends to move downward rather than radially around the emitter, as predicted numerically in the axisymmetrical three-dimensional domain for sand (Fig. 9b,d). These results are also summarized in Fig. 12. For both soils, the WUE decreased as the number of holes decreased.

Cumulative RWU increased significantly in both soils when the compensated RWU model was used (Fig. 11cd). For silt, while compensated RWU with a smaller number of holes was much smaller than that for the emitter with more holes at earlier time, they were almost the same at the end of simulation. This can be also seen in the computed WUE for compensated RWU for silt for both model plants (Fig. 12). As

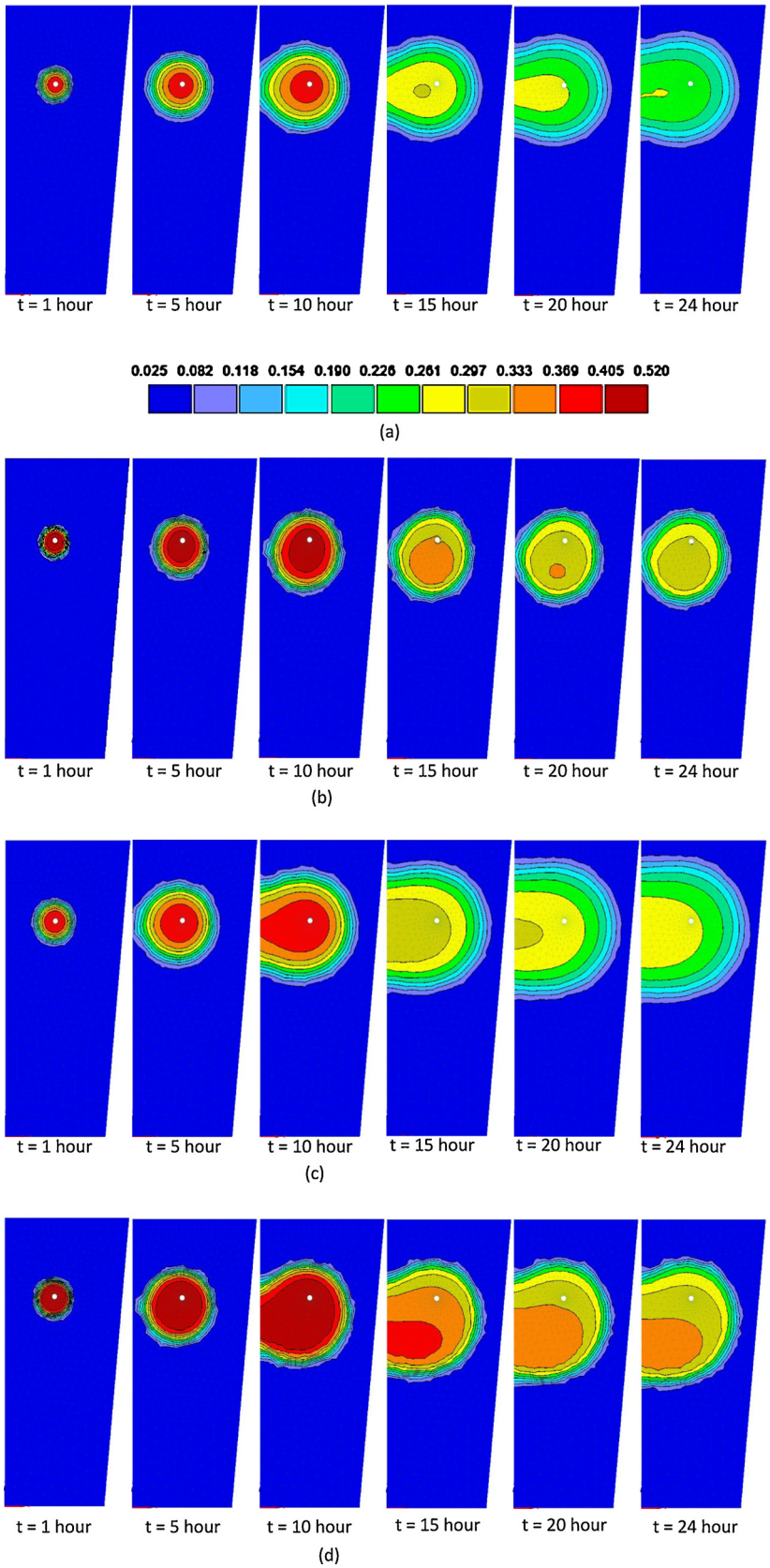

Fig. 9. Water contents in the axisymmetric three-dimensional flow domain simulated using HYDRUS with the calibrated van Genuchten-Mualem parameters. (a) silt with the 1-cm inlet pressure head, (b) sand with the 1-cm inlet pressure head, (c) silt with the 5-cm inlet pressure head, and (d) sand with the 5-cm inlet pressure head.

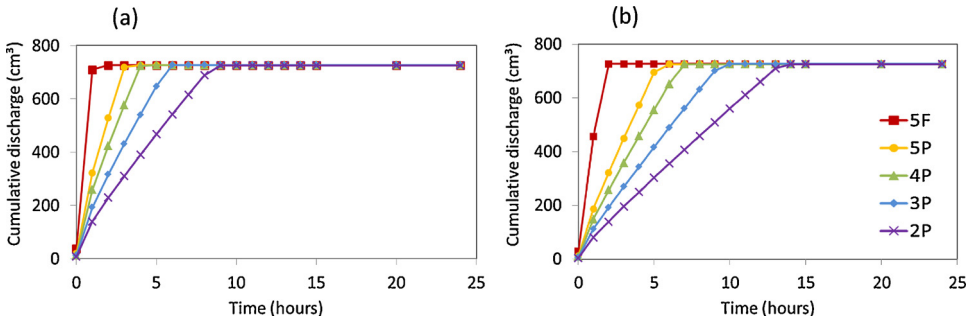

Fig. 10. Cumulative infiltration computed for different ring-shaped emitters using HYDRUS with the optimized soil hydraulic parameters for silt (a) and sand (b) under tomato cultivation.

water was slowly discharged from the emitter with less holes, RWU slowly increased. This implies that reducing the number of holes does not affect the amount of water available for plant root uptake over 24 h in silt. When the compensated RWU model was used for sand, the general trend was the same as for the uncompensated RWU model, except that cumulative compensated RWU was much larger.

The effect of preceding irrigations was then assessed for different emitter designs by computing compensated cumulative RWU over 21 days (i.e., 504 h), during which seven irrigation cycles were considered (Fig. 13). Cumulative compensated RWUs after 21 days for different emitter designs were almost the same for silt. On the other hand, for sand, cumulative compensated RWU is strongly affected by the emitter design. For 5 F, unlike the 24-hour simulation case shown in Fig. 11, cumulative RWU starts being reduced after 8 days, while cumulative RWUs computed for the emitters with fewer holes continuously increase. At the end of the simulation, simulated cumulative RWU for 3 P reaches the highest value, and thus the highest WUE, among different evaluated designs. For 5 F, the water application rate was too high for plant roots to uptake. As a result, there was a significant amount of water lost to deep percolation. For the emitters with fewer holes, the water application rate was smaller and consequently that there was much less water lost to deep percolations even for sand. In summary. these simulation results confirm that the number of holes can be reduced to 2 or 3 regardless of the soil types considered in this study.

4. Summary and conclusions

The experimental results showed that water moved radially around the emitter in silt, while downward water movement was dominant in sand when water was applied using the buried ring-shaped emitter. The difference in the flow pattern can be attributed to the difference in the macroscopic capillary length of the soil, which can be interpreted as a measure of the contribution of capillarity as opposed to gravity's effect on unsaturated water movement. HYDRUS, a model simulating variably-saturated water flow in porous media, was then calibrated using the experimental data collected from the experiments with the 1-cm inlet pressure head. The calibrated soil hydraulic parameters were used to simulate changes in soil water contents (SWCs) for the experiments with the 5-cm inlet pressure head. While SWCs were predicted well for silt, SWCs above the buried emitter were overestimated and those

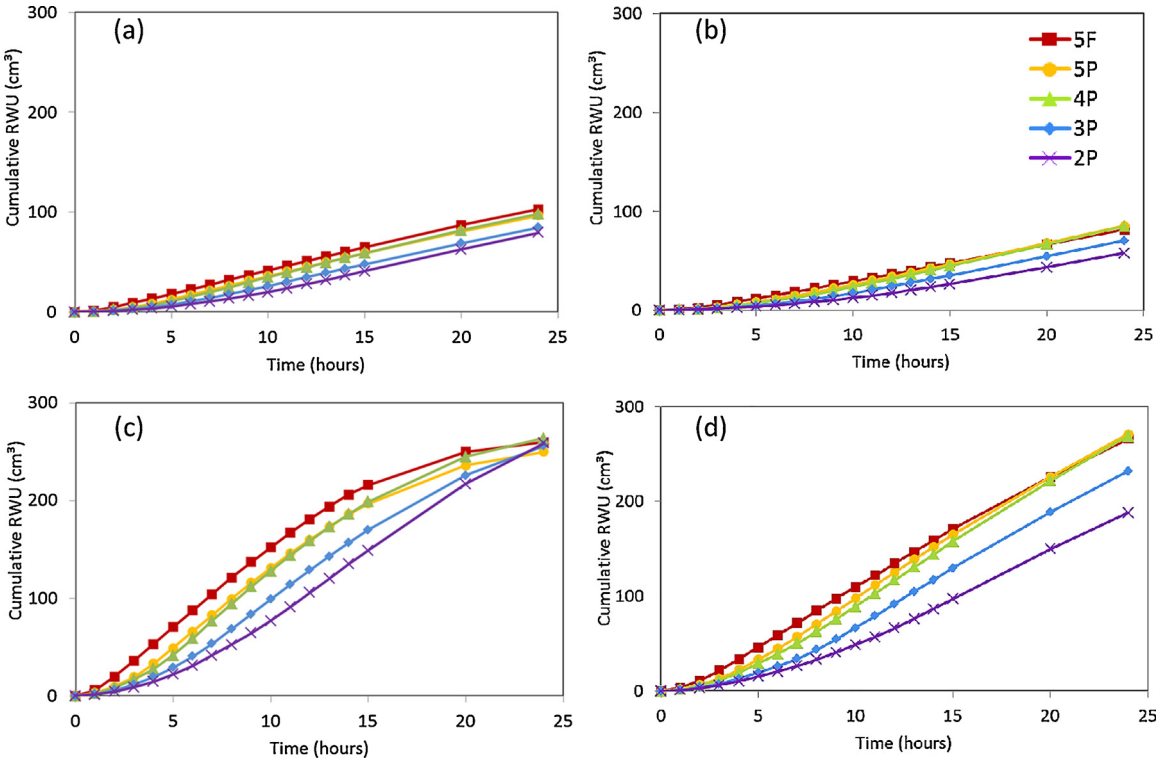

Fig. 11. Uncompensated (a and b) and compensated (c and d) cumulative root water uptake computed for the buried ring-shaped emitters of different designs using HYDRUS with the optimized soil hydraulic parameters for both silt (a and c) and sand (b and d) under tomato cultivation.

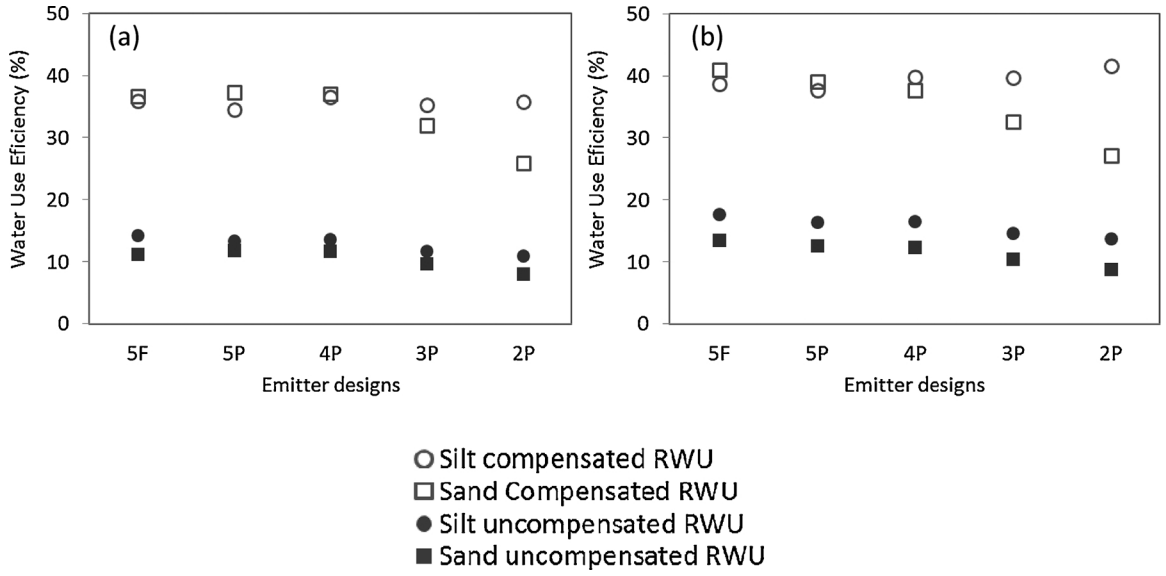

Fig. 12. Water use efficiency (WUE) computed for emitters of different designs after 24 h for the 10-h water application and tomato (a) and strawberry (b) cultivation using compensated and uncompensated root water uptake models in HYDRUS.

directly below the emitter were underestimated for sand. Although the fitted saturated hydraulic conductivity for sand was too small, this result indicates that downward water movement was predominant, suggesting the occurrence of preferential flow.

With the optimized soil hydraulic parameters, HYDRUS was used to investigate the effects of alternative emitter designs on the spatial extent of the wetted volume around the buried emitter during the subsurface water application. Had the spatial distribution of the SWC been non-uniform, some parts of the plant root system would have been stressed, resulting in the reduction in root water uptake. In this analysis, plant root water uptake was therefore used as an indirect, quantitative proxy measure to assess the non-uniformity in the spatial extent of the wetted volume around the emitter. Two model plants, tomato and strawberry, were considered because of their contrasting root distributions. Both uncompensated and compensated RWU were then computed. While the former was used to assess the non-uniformity in the spatial extent of the wetted volume, the latter was used to investigate whether such non-uniformity had any effect on plant root water uptake.

In addition to the original 5-hole emitter that was fully covered by a permeable textile, four separate emitter designs with a different number of holes were analyzed. The new emitter proposed in this study was

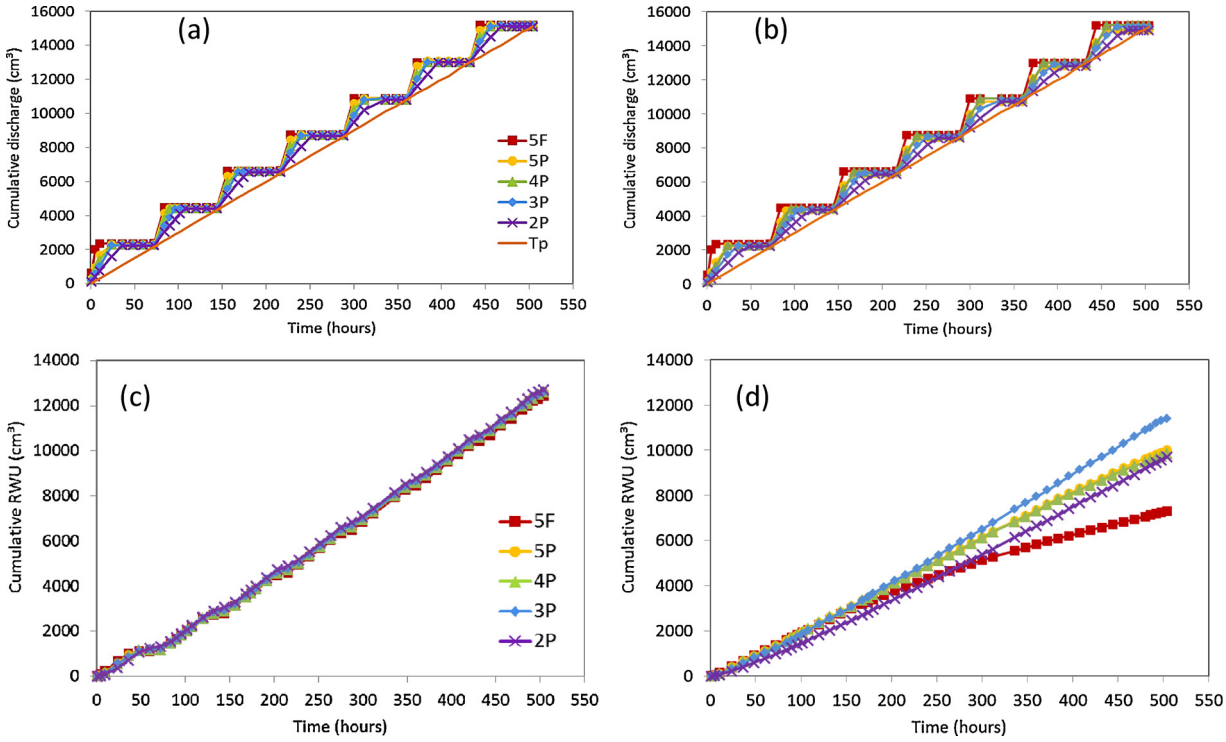

Fig. 13. Cumulative infiltration computed for different ring-shaped emitters using HYDRUS with the optimized soil hydraulic parameters for silt (a) and sand (b) under tomato cultivation with seven irrigation cycles over 21 days. Compensated (c and d) cumulative root water uptake computed during the same duration of 21 days for both silt (c) and sand (d).

only partially covered by the textile around the holes to simplify the maintenance of the emitter. Numerical simulations with these alternative emitter designs showed that the lower number of holes did not significantly affect uncompensated RWU in silt. However, in sand, cumulative uncompensated RWU decreased when the emitters with reduced number of holes were used in the initially dry soil, suggesting non-uniformity in the wetted volume. The non-uniformity in the wetted volume in silt for the emitter with fewer holes was not significantly different because water moved radially from the emitter, diminishing the effect of the spatial hole configuration. For sand, on the other hand, the non-uniformity in the wetted volume was larger, as indicated by uncompensated RWU.

Such non-uniformity in the wetted volume does not affect the long-term performance of the ring-shaped emitter with fewer holes even for sand because of the slow discharge rate. Simulated compensated RWU for both model plants revealed that reducing the number of holes in sand gradually increased RWU as slowly infiltrating water allowed plant roots to uptake water continuously. This may not be beneficial when considering the diurnal water uptake pattern of plants, when higher RWU occurs in daylight time.

These results show that, regardless of the soil type, reducing the number of holes and changing the covering method may result in a much better water use efficiency and easier maintenance. Overall, this study demonstrates that HYDRUS is a useful tool for analyzing soil water dynamics around the buried ring-shaped emitter during the subsurface water application.

Acknowledgments

This study was partially supported by JSPS Grant-in-aid Scientific Research program (17H03885). We would like to thank Dr. Satyanto K.Saptomo and Prof. Budi Indra Setiawan of Bogor Agricultural Univesity for letting us to use their ring-shaped emitter. The authors greatly acknowledge constructive and critical comments of two anonymous reviewers and the editor that helped to improve the manuscript.

References

Bufon, V.B., Lascano, R.J., Bednarz, C., Booker, J.D., Gitz, D.C., 2012. Soil water content on drip irrigated cotton: comparison of measured and simulated values obtained with the hydrus 2-D model. Irrig. Sci. 30, 259–273. https://doi.org/10.1007/s00271-011-0279-z.

Cote, C.M., Bristow, K.L., Charlesworth, P.B., Cook, F.J., Thorburn, P.J., 2003. Analysis of soil wetting and solute transport in subsurface trickle irrigation. Irrig. Sci. 22, 143–156. https://doi.org/10.1007/s00271-003-0080-8.

Dekker, L.W., Ritsema, C.J., 1994. How water moves in a water repellent sandy soil: 1. Potential and actual water repellency. Water Resour. Res. 30, 2507–2517. https://doi.org/10.1029/94WR00749.

El-Nesr, M.N., Alazba, A.A., Šimůnek, J., 2014. HYDRUS simulations of the effects of dual-drip subsurface irrigation and a physical barrier on water movement and solute transport in soils. Irrig. Sci. 32, 111–125. https://doi.org/10.1007/s00271-013-0417-x.

Feddes, R.A., Kowalik, P.J., Zaradny, H., 1978. Simulation of Field Water Use and Crop Yield. John Wiley & Sons, New York.

Gärdenäs, A.I., Hopmans, J.W., Hanson, B.R., Šimůnek, J., 2005. Two-dimensional modeling of nitrate leaching for various fertigation scenarios under micro-irrigation. Agric. Water Manage. 74, 219–242. https://doi.org/10.1016/j.agwat.2004.11.011.

Ghazouani, H., M'Hamdi, B.D., Autovino, D., Mguidiche Bel Haj, A.M., Rallo, G., Provenzano, G., Boujelben, A., 2015. Optimizing subsurface dripline installation depth with Hydrus 2D/3D to improve irrigation water use efficiency in the central Tunisia. Int. J. Metrol. Qual. Eng. 6, 1–9. https://doi.org/10.1051/ijmqe/2015024.

Jury, W.A., Horton, R., 2004. Soil Physics, sixth ed. John Wiley & Sons, Inc., New York.

Kandelous, M.M., Šimůnek, J., 2010a. Comparison of numerical, analytical, and empirical models to estimate wetting patterns for surface and subsurface drip irrigation. Irrig. Sci. 28, 435–444. https://doi.org/10.1007/s00271-009-0205-9.

Kandelous, M.M., Šimůnek, J., 2010b. Numerical simulations of water movement in a subsurface drip irrigation system under field and laboratory conditions using HYDRUS-2D. Agric. Water Manage. 97, 1070–1076.

Kandelous, M.M., Šimůnek, J., van Genuchten, M.T., Malek, K., 2011. Soil water content distributions between two emitters of a subsurface drip irrigation system. Soil Sci. Soc. Am. J. 75, 488. https://doi.org/10.2136/sssaj2010.0181.

Kandelous, M.M., Kamai, T., Vrugt, J.A., Šimůnek, J., Hanson, B., Hopmans, J.W., 2012. Evaluation of subsurface drip irrigation design and management parameters for alfalfa. Agric. Water Manage. 109, 81–93. https://doi.org/10.1016/j.agwat.2012.02.009.

Lazarovitch, N., Šimůnek, J., Shani, U., 2005. System-dependent boundary condition for water flow from subsurface source. Soil Sci. Soc. Am. J. 69, 46–50.

Lazarovitch, N., Warrick, A.W., Furman, A., Šimůnek, J., 2007. Subsurface water distribution from drip irrigation described by moment analyses. Vadose Zone J. 6, 116. https://doi.org/10.2136/vzj2006.0052.

Marquardt, D.W., 1963. An algorithm for least-squares estimation of nonlinear parameters. SIAM J. Appl. Math. 11, 431–441.

Naglič, B., Kechavarzi, C., Coulon, F., Pintar, M., 2014. Numerical investigation of the influence of texture, surface drip emitter discharge rate and initial soil moisture condition on wetting pattern size. Irrig. Sci. 32, 421–436. https://doi.org/10.1007/s00271-014-0439-z.

Provenzano, G., 2007. Using HYDRUS-2D simulation model to evaluate wetted soil volume in subsurface drip irrigation system. J. Irrig. Drain. Eng. 133, 342–349.

Radcliffe, D., Šimůnek, J., 2010. Taylor and francis group, boca raton, FL. Soil Physics With HYDRUS: Modeling and Applications. CRC Press.

Saefuddin, R., Setiawan, B.I., Saptomo, S.K., Mustaningsih, P.R.D., 2014. Performance analysis of emitter ring irrigation system. J. Irig. 9, 63–74. https://doi.org/10.13140/RG.2.1.1102.6647. in Indonesian with English Abstract.

Shani, U., Xue, S., Gordin-Katz, R., Warrick, A.W., 1996. Soil limiting flow from subsurface emitters. I: pressure measurements. J. Irrig. Drain. Eng. 122, 291–295.

Shani, U., Ben-Gal, A., Tripler, E., Dudley, L.M., 2007. Plant response to the soil environment: an analytical model integrating yield, water, soil type, and salinity. Water Resour. Res. 43, 1–12. https://doi.org/10.1029/2006WR005313.

Šimůnek, J., Hopmans, J.W., 2009. Modeling compensated root water and nutrient uptake. Ecol. Modell. 220, 505–521. https://doi.org/10.1016/j.ecolmodel.2008.11.004.

Šimůnek, J., van Genuchten, M.Th., Šejna, M., 2011. The HYDRUS Software Package for Simulating Two- and Three-Dimensional Movement of Water, Heat, and Multiple Solutes in Variably-Saturated Media, Technical Manual, Version 2.0. PC Progress, Prague, Czech Republic pp. 258.

Šimůnek, J., van Genuchten, M.Th., Šejna, M., 2016. Recent developments and applications of HYDRUS computer software packages. Vadose Zone J. 6, 1–25. https://doi.org/10.2136/vzj2016.04.0033.

Skaggs, T.H., Trout, T.J., Šimůnek, J., Shouse, P.J., 2004. Comparison of HYDRUS-2D simulations of drip irrigation with experimental observations. J. Irrig. Drain. Eng. 130, 304–310. https://doi.org/10.1061/(ASCE)0733-9437(2004)130:4(304).

Sumarsono, J., Setiawan, B.I., Subrata, I.D.M., Waspodo, R.S.B., Saptomo, S.K., 2018. Ring-typed emitter subsurface irrigation performances in dryland farmings. Int. J. Civ. Eng. Technol. 9, 798–806.

van Genuchten, M.Th., 1980. A closed form equation for predicting the hydraulic conductivity of unsaturated soils. Soil Sci. Soc. Am. J. 44, 892–898.

van Genuchten, M.T., Leij, F.J., Yates, S.R., 1991. The RETC Code for Quantifying the Hydraulic Functions of Unsaturated Soils. Environ. Research. Lab., United States, pp. 93. https://doi.org/10.1002/9781118616871.

Vrugt, J.A., Van Wijk, M.T., Hopmans, J.W., Šimunek, J., 2001. One-, two-, and three-dimensional root water uptake functions for transient modeling. Water Resour. Res. 37, 2457–2470. https://doi.org/10.1029/2000WR000027.